Hydrol. Earth Syst. Sci. Discuss., 10, 8841–8874, 2013
www.hydrol-earth-syst-sci-discuss.net/10/8841/2013/
doi:10.5194/hessd-10-8841-2013

Hydrology and Earth System Sciences
Open Access
Discussions

Indirect downscaling of global circulation model data based on atmospheric circulation and temperature for projections of future precipitation in hourly resolution

F. Beck and A. Bárdossy

University of Stuttgart, Institute for Modelling Hydraulic and Environmental Systems, Stuttgart, Germany

Received: 19 June 2013 – Accepted: 3 July 2013 – Published: 8 July 2013

Correspondence to: F. Beck (ferdinand.beck@iws.uni-stuttgart.de)

Published by Copernicus Publications on behalf of the European Geosciences Union.

Abstract

Many hydraulic applications like the design of urban sewage systems require projections of future precipitation in high temporal resolution. We developed a method to predict the regional distribution of hourly precipitation sums based on daily mean sea level pressure and temperature data from a Global Circulation Model. It is an indirect downscaling method avoiding uncertain precipitation data from the model. It is based on a fuzzy-logic classification of atmospheric circulation patterns (CPs) that is further subdivided by means of the average daily temperature. The observed empirical distributions at 30 rain gauges to each CP-temperature class are assumed as constant and used for projections of the hourly precipitation sums in the future. The method was applied to the CP-temperature sequence derived from the 20th century run and the scenario A1B run of ECHAM5. According to ECHAM5, the summers in southwest Germany will become progressively drier. Nevertheless, the frequency of the highest hourly precipitation sums will increase. According to the predictions, estival water stress and the risk of extreme hourly precipitation will both increase simultaneously during the next decades.

1 Introduction

State of the art in the design of urban sewage systems is the application of hydraulic models. The dimensioning of channels and reservoirs is based on the results of numerical discharge simulations, e.g. the frequency of backwater events in the channel network. As a major input hydraulic channel models require precipitation data of appropriate resolution, which depends on the concentration time of the channel network (Berne et al., 2004). Since sewage systems are very fast reacting systems, a resolution of one hour or shorter is required.

Frequently, observed precipitation time series are used as input, implying the assumption that precipitation from the past is representative for the future. Under chang-

HESSD
10, 8841–8874, 2013

ing climatic conditions, however, this assumption is the less and less true the further one looks into the future. Since sewage systems are very long lasting investments, changes in precipitation during their lifespan have to be considered in the design.

Main source of information on future climate conditions are Global Circulation Models (GCMs). While the various GCMs agree on an increase of surface temperature, predictions for precipitation exhibit high spread among the models. The complex physics of precipitation genesis results in high spatial and temporal heterogeneity, which cannot be represented to full extend by the GCMs.

On the global scale an increase in precipitation is expected during the 21st century due to enhanced evaporation under warmer climatic conditions. The GCMs used in IPCC's fourth assessment report predict a global precipitation increase of 1 to 3 % $^{\circ}C^{-1}$ of global warming (Held and Soden, 2006). Wentz et al. (2007) estimated the relation between average global temperature and total global precipitation volume from satelite observations and found a rate of 7.4 % (with a possible error of ± 2.6 %) $^{\circ}C^{-1}$. The rate is in aggreement with the Clausius–Clapeyron relation which states that the moisture capacity of the air increases by about 7 % $^{\circ}C^{-1}$. Over the oceans evaporation is mainly governed by the moisture capacity. A warmer atmosphere can evaporate and carry more water, which has to fall down somewhere so that the mass balance is fullfilled.

Regional changes in precipitation, however, differ from the Clausius–Clapeyron increase rate since they are not only governed by the potential evaporation, but also by changes in other factors, e. g. atmospheric circulation or soil moisture. In an extensive study comparing several runs of the AM3P from Met Office Hadley Centre, UK, Kendon et al. (2010) evaluated the effects of global changes in different climatic factors on regional precipitation. According to the model, one of the key factors for most parts of Europe is soil moisture depletion, leading to drier conditions during summer months when atmospheric temperature is rising (Kendon et al., 2010).

In observed time series regional deviations from the Clausius–Clapeyron relation have been found, too. In central Europe during the second half of the 20th century temperature had been increasing, but an increase in precipitation volume could not

HESSD
10, 8841–8874, 2013

be observed. An increase during winter months was balanced by a decrease during summer (Hundecha and Bárdossy, 2005). Simultaneously, daily precipitation extremes had become more pronounced (Hundecha and Bárdossy, 2005), indicating a shift in the distribution. Both trends are confirmed by climate model runs and are predicted to continue in the future, e. g. by the PRUDENCE ensemble study of 19 combinations of Global and Regional Circulation Models (RCMs). (See Déqué et al., 2007 for the seasonal shift, Fowler et al., 2007 for the extremes.)

Most studies analyzing GCM output deal with monthly or daily precipitation sums. Although GCMs exhibit a temporal resolution of up to 30 min, sub-daily values are generally discarded. Due to the limited spatial resolution of GCMs, convective events, which are responsible for the highest precipitation intensities, can only be modeled conceptually (Trenberth et al., 2003). The parametrization of convection, however, is still problematic (Guichard et al., 2004). Hence, it is assumed that model errors are highest in the shortest time steps, where convection plays a major role. To avoid the application of uncertain GCM-data, climate predictions of sub-daily precipitation amounts are generally based on spatial-temporal downscaling of daily values.

Downscaling can be done dynamically by nesting an RCM with higher resolution but limited spatial extend in the global model and/or by statistical methods. While dynamical downscaling is based on physical information finding its expression in the equations of the RCM, statistical downscaling is merely based on the statistical relation of precipitation on different scales, e.g. of daily and sub-daily resolution. In general, statistical downscaling methods are calibrated with data from past time observations. The established relation is then applied to the GCM data of the future. Nguyen et al. (2007) developed a downscaling scheme that links daily and hourly precipitation extremes by a multiple linear regression approach that takes spatial correlations into account. Another possibility are cascade models that link precipitation of different spatial-temporal resolution by the multi-fractal scaling characteristics (e.g. Molnar and Burlando, 2005). As they exhibit a low number of parameters and an easy model fit, they are frequently used for downscaling applications. Groppelli et al. (2011) for example use a random

HESSD
10, 8841–8874, 2013

cascade model for spatial downscaling of daily GCM precipitation sums. The grid cells of the GCM are about 200 km^2, the target scale of the catchment model is 2 km × 2 km. Willems and Vrac (2011) compare several other downscaling methods, e.g. the delta change method and the analogues method. In the delta change method, the absolute precipitation values of the GCM are discarded, only the trend signal (the delta change) is kept, which is used to modify locally observed distributions of the past. Lenderink et al. (2007) examine the effect of the delta change method on river discharges simulated in a hydrological model. While the average discharges are similar to the discharges calculated directly from RCM precipitation, the extremes are much higher when delta changed data is applied. The analogues method does not use any precipitation data from the GCM, but uses observed precipitation from past days as predictions for the future. The choice of the past days that are assigned to the GCM output is based on a similarity measure, e.g. of the predicted atmospheric circulation.

The application of statistical downscaling in climate change studies implies the assumption that the relation between the scale of the GCM and the target scale is constant over time. Concerning precipitation, the assumption becomes problematic if the temporal target resolution is shorter than one day, since there is strong evidence that global warming affects the relation between daily and sub-daily precipitation sums. An examination based on data from several hundred rain gauges in South West Germany revealed changes in the temporal scaling. In portion of the daily sum that can fall within one hour has been increasing during the second half of the 20th century. This increase concerns the extremes as well as average events (Beck, 2013, 153–157).

For De Bild, Netherlands, it was found that the 99% quantile of hourly preciption amounts increases by the double of the Clausius–Clapeyron relation if the atmospheric temperature exceeds 14 °C, while the 99% quantile of daily sums grows by the Clausius–Clapeyron rate of 7 % °C^{-1} (Lenderink and van Meijgaard, 2008). It proves that the relation between hourly and daily precipitation is temperature-sensitive and, therefore, will react on global warming. A sucessing study revealed similar behaviour in Hong Kong, under subtropical climatic conditions (Lenderink et al., 2011). Thus, the findings

HESSD
10, 8841–8874, 2013

are not limited to temperate climate, but might probably indicate a universal property of precipitation. Trenberth et al. (2003) predicted such a behaviour, called "super Clausius–Clapeyron", for convective precipitation events assuming a positive feedback effect at the onset of condensation: The higher absolute moisture content of a warmer atmosphere leads to a stronger latent heat release during condensation, which in turn reinforces the convective uplift responsible for condensation (Trenberth et al., 2003).

If a constant relation is assumed between daily and hourly precipitation, super Clausius–Clapeyron behavior is ignored resulting in a problematic underestimation of extreme hourly precipitation frequencies. Therefore, any temporal downscaling method used in climate change studies requires additional information to represent changes in the relation of daily to sub-daily precipitation.

This paper describes a GCM downscaling scheme that takes information on atmospheric circulation and temperature into account. The output are not time series but the expected future distribution of hourly precipitation which, in a next step, can be used as basis for stochastic time series simulation. It is an indirect method which does not use any GCM precipitation data. Instead, it relies on predictions of the mean sea level pressure (MSLP) and atmospheric temperature, which are considered as more reliable (see for example Kendon and Clark, 2008). The downscaling scheme is presented by an application on the regional scale, namely the federal state of Baden-Württemberg in the southwest of Germany (about 35 000 km^2).

Outline

In the next section the methodology of the CP classification system is explained and how it is used for downscaling purposes.

In section three the observed CP sequence between 1958 to 2003 is analyzed. CPs which frequently lead to high hourly precipitation sums are identified and trends in the CP-sequence estimated. It is investigated how the CPs react on temperature.

HESSD
10, 8841–8874, 2013

Section 4 gives a prognosis on the CP sequence until 2060 based on the Global Circulation Model ECHAM5. Expectations for the yearly precipitation sum and the probability for extreme hourly precipitation sums are derived from the CP sequence.

The paper concludes by an estimation of the reliability of the projected trends in hourly precipitation and a short outlook of how the result can be incorporated in synthetic time series generation.

2 Methodology

2.1 Fuzzy rule based CP classification

The proposed downscaling method is based on a circulation pattern (CP) classification of the atmospheric flow field. The CPs result from an objective and automated classification which does not require any expert judgment. It follows the method described by Bárdossy (2010), expect for modifications concerning the objective function. The CPs are further subdivided into temperature classes to take the temperature sensitivity of the relation between hourly and daily rainfall depths into account.

The classification is performed by a fuzzy rule system based on normalized mean sea level pressure (MSLP) anomalies derived from the NCEP/NCAR reanalysis (Kistler et al., 2001). The temporal resolution is 2.5° by 2.5°. Based on the pressure anomalies, five fuzzy states are defined:

1. large positive anomalies
2. medium positive anomalies
3. medium negative anomalies
4. large negative anomalies
5. arbitrary.

HESSD
10, 8841–8874, 2013

The fuzzy rule set defining the n_{cp} CPs specifies the required fuzzy state for each of the grid points. It can be described by a matrix:

$$\mathbf{V} = v(i,j); \quad i = 1,\ldots n_{pts}; \quad j = 1,\ldots n_{cp}. \tag{1}$$

The definition of one CP class j consists of the state index v = (1, 5) to each grid point i of the n_{pts} grid points in the MSLP-anomalies field over Europe and the northern Atlantic Ocean. The state "arbitrary" is assigned to all points that are indifferent to the respective weather type definition. For each day the current anomaly field is compared with the CP-defining fuzzy rule set. The CP with the highest resemblance, resulting in the highest degree of fulfillment (DOF) of the fuzzy rule, is chosen as the CP of the day. The number of CPs is set to n_{cp} = 12. All days that cannot be assigned to any of the the twelve predefined CPs, because the DOF is below a certain threshold, are assigned to the additional class "CP99".

2.2 Definition of the rule set

The rule set which forms the classification system is not predefined, but found by a stochastic optimization. A Simulated Annealing algorithm (Aarts and van Laarhoven, 1989) arbitrarily chooses grid points, assigns fuzzy anomaly states and evaluates the performance of the resulting classification system by an objective function O, the target of the optimization. The optimal classification is found if the CPs differ as much as possible in their statistical properties, which is measured by O.

Since the classification will be used to examine the effect of climate change on sub-daily precipitation, the objective function is designed to detect differences in the distribution of hourly precipitation amounts. According to the sketch in Fig. 1, the CP classification is optimal when the distribution of 1 h precipitation amounts of all days belonging to the same CP differs the most from the climatic average. The difference is measured by the variable χ^2 which is equal to the sum of the squared residuals in

HESSD
10, 8841–8874, 2013

relative frequency $h_i(j)$ between the histogram class j for all days belonging to one CP i and the same histogram class for the climatic average $h_{\text{clim}}(j)$ without classification:

$$\chi^2 = \sum_{i=1}^{n_{\text{cp}}} \sum_{j=1}^{k} (h_i(j) - h_{\text{clim}}(j))^2 \rightarrow \max! \quad (2)$$

(χ^2 is equal to the sum of the squared lengths of the arrows in Fig. 1.)

The limits of the $j \in [1,k]$ histogram classes are defined by the empirical quantiles to predefined CDF values. To shift the focus towards high precitation amounts, the classes are not equidistant in CDF but smaller for higher CDFs. The upper limits of the histogram classes are $F^{-1}(0.6)$, $F^{-1}(0.8)$, $F^{-1}(0.9)$, $F^{-1}(0.95)$, $F^{-1}(0.98)$, $F^{-1}(0.99)$ and $F^{-1}(1.0)$, which means that the last class is open to the right. The CDFs are calculated from all wet hours with no less than 0.1 mm of precipitation. The histograms are calculated for two seasons, from September to April and from May to August to account for convective precipitation enhancement during summer months.

The difference of the CPs to the climatic average in hourly rainfall frequency is taken as a second part of the objective function O to distinguish between wet and dry CPs.

Data basis for the histograms calculation is a homogeneous set of 30 close to complete hourly precipitation time series from 1991 to 2003. The locations of the rain gauges are spread all over Baden-Württemberg (see Fig. 2). To make the rainfall depths of different stations comparable, histogram classes are defined at each station individually according to the local CDF. Then the relative frequency of each class of each CP is averaged over all stations.

2.3 Temperature subdivision

The 12 CP classes are further subdivided according to the average observed daily air temperature at 156 measurement stations in Baden-Württemberg, which is seen as a representation of the atmospheric temperature. The subdivision is made by the observed temperature CDF to each CP. The 20 % of days with the coldest average

HESSD
10, 8841–8874, 2013

temperature in each CP class are declared “cold”, the next 20 % cool, followed by “avg”, “warm” and “hot” conditions. To avoid seasonal effects, the quantiles are calculated on basis of anomalies from the average yearly cycle.

2.4 CP-temperature classification as downscaling tool

The CP-temperature classification has two results. First the sequence of CP-temperature classes and second, the empirical distribution of hourly precipitation sums at the 30 precipitation stations of each CP-temperature combination in each of the two seasons (September to April and May to August). The spatial-temporal downscaling effect of the classification lies in the empirical distributions: information on hourly precipitation values on a regional scale is associated with daily information of the large scale atmospheric circulation and atmospheric temperature.

The CP defining fuzzy rule set can be applied to gridded daily MSLP data of any GCM. The only condition is that the spatial resolution is comparable to the resolution of the NCEP/NCAR reanalysis. In this study it is applied to data from two runs of ECHAM5 from the Max-Planck Institute in Hamburg, Germany (Roeckner et al., 2003). The temperature subdivision is based on the average daily temperature of the grid cell over the study region.

Thus, pressure and temperature data are transformed into a time series of daily CP-temperature classes. If it is assumed that the distribution of hourly precipitation sums to each CP-temperature class in each season (September to April and May to August) does not change over time, the observed statistics during the calibration period from 1991 to 2003 can be used to derive hourly precipitation statistics from the CP-temperature sequence of the GCM run. The average observed cumulated histogram frequencies are seen as a prediction of the CDF, the observed rainfall frequency as the expected rainfall probability. Taking the CP-temperature sequence of one target year from the GCM run, the predicted yearly distribution is calculated as the weighted average of the distribution to each CP-temperature class. The weights are the relative frequencies of the CP-temperature classes in each of the two seasons. In a next step,

HESSD
10, 8841–8874, 2013

other statistics can be derived from the expected distributions of the target year, e.g. the exceedance frequency of each histogram limit or the expected yearly precipitation sum.

3 CP classification according to NCEP/NCAR reanalysis data

3.1 CPs with potential for high hourly precipitation sums

The maps in Fig. 3 show the average pressure anomalies according to the NCEP-NCAR data set of all days belonging to three CPs which frequently lead to high hourly precipitation sums. CP2 is a high pressure situation with generally weak atmospheric exchange. CP7, with the low pressure center over South of Norway, generates western to northwestern fluxes. CP11 generates northern fluxes between the high pressure zone over the Atlantic ocean and the low pressure zone over eastern Europe. It might seem surprising in first respect that CP2 is among the CPs with highest potential for intensive precipitation (Fig. 3a) since high pressure situations generally lead to dry conditions. If it rains, however, convective events can provoke high intensities, especially during summer months.

Figure 4 displays the relative exceedance frequencies of the 95 and 99 % quantile of all wet hour precipitation amounts. In average over all CPs and both seasons the frequency is 5 %, respectively 1 % during the calibration periode from 1991 to 2003. High intensities are generally more frequent during summer months. The highest intenstities are mainly produced by convective precipitation events. In winter convective events are bound to turbulent mixing at cold fronts. During summer months the increased solar heating is an additional driving force for convection or even triggers events that are not bound to an approaching front. Therefore, the estival increase in the 95 and 99 % quantile exceedance frequencies indicates the influence of convection. The anticyclonic CP2 exhibits an elevated potential for high hourly sums only during summer months, while the frequency of CP11 with turbulent northern fluxes is among the

HESSD
10, 8841–8874, 2013

highest during both seasons. CPs with westerly fluxes as CP7 are less influenced by convective intensity enhancement and show the lowest increase in the 95 and 99 % quantile exceedance frequencies during summer months.

3.2 Changes in the CP sequence

An analysis of the occurrence frequencies reveals changes in the CP sequence (Fig. 5). For this purpose the CPs were grouped according to their meteorological characteristics. The first line of Fig. 5 shows the frequency of anticyclonic CPs between 1958 to 2004 according to the NCEP/NCAR reanalysis MSLP anomalies. During the CP calibration period from 1991 to 2003, one of the anticyclonic CPs occurred on 35.6 % of all days, but only 17.5 % of all rainy hours at the 30 rain gauges used for calibration were counted during that time. The second line in Fig. 5 displays the absolute frequency of cyclonic CPs. From 1991 to 2003, one of these CPs occurred on 30.0 % of all days. They are responsible for 55.4 % of all hours with non-zero precipitation.

Potential trends in the CP sequence between 1958 and 2004 (NCEP/NCAR) are quantified by linear regression and marked by a line in Fig. 5. The significance of the regression is evaluated by a two sided hypothesis test. The value of "alpha" below the equation of the regression function is the significance of rejecting the hypothesis that the slope of the true regression line is zero.

Figure 5 suggest that the atmospheric circulation has shifted between 1958 and 2004. The number of days with anticyclonic CPs has increased, during the summer months by almost two days in every five years between 1958 to 2004, the number of days with cyclonic CPs decreased. Taking $\alpha = 5\,\%$ as a limit, there is a significant increasing trend in high pressure situations in both seasons and a decreasing trend in low pressure situations from September to April.

HESSD
10, 8841–8874, 2013

3.3 Reaction of temperature

The effect of the temperature subdivision on the empirical distribution of each CP is demonstrated by the example of CP2, CP7 and CP11. It is tested by the hourly precipitation frequency with a threshold of 0.1 mm and the exceedance frequency of the 95 and 99 % quantile refering to all wet hours ($R \geq 0.1$ mm) of the respective CP.

All three tested CPs react on temperature with a particularly strong signal during summer months. From May to August there is a pronounced drop in precipitation frequency with increasing temperature (right column of Fig. 6). The exceedance frequency of the 95 % quantile is more than two times higher during "hot" days than during "cold" days in any of the CPs (right column of Fig. 7). It seems that the highest hourly sums are affected the most. The differences between "cold" and "hot" days in the 99 % quantile are far more pronounced than in the 95 % quantile (right column of Fig. 8), going up to an increase by a factor of 12 for CP11. From May to August the elevated exceedance frequency of the 99 % quantile during days of CP7 and CP11 overcompensates the decrease in overall precipitation frequency. Refered to all hours, the highest hourly sums occur more often – even if it rains more rarely than average on "hot" days.

During summer all three CPs react in the same way, although not to the same extend. Higher temperatures lead to fewer rainy hours, but shift the distribution towards higher precipitation amounts. Between September and April, the reaction on temperature is less pronounced and more varying among the CPs. For CP2 the rainfall frequency is slightly increasing, for CP7 and CP11 more or less constant (left column of Fig. 6). During days of CP2 and CP7 high values are more frequent for higher temperature (left column of Figs. 7 and 8). During CP11 the exceedance frequency of the 95 % quantile is constant (Fig. 7e). The exceedance frequency of the 99 % quantile is the higher the more the temperature deviates from the average (Fig. 8e).

The seasonal differences indicate that the reaction to atmospheric temperature depends on the precipitation genesis. Due to the higher solar radiation, convective events are predominant between May and August and that is when the temperature classifi-

HESSD
10, 8841–8874, 2013

cation has the strongest effect on the frequency of high hourly precipitation amounts. The findings are in agreement with physical considerations. Trenberth (1999) states that an increase in atmospheric temperature should lead to fewer but more intensive rainfall events due to the stronger convective uplift and the higher moisture capacity of a warmer atmosphere. Thus, although the classification is merely based on statistical properties, it leads to physically sound results.

Nevertheless, the CP and temperature classification is not able to completely separate the effects of higher atmospheric temperature and changes in the atmospheric circulation. The atmospheric temperature over central Europe is not only a measure of the moisture capacity and the potential strength of convective uplift, but also an indicator of the origin of the arriving air masses. Since the days belonging to one CP class do not have completely identical pressure maps, the flow field of each CP can vary to a certain extend. Lower temperatures in winter for example may indicate a shift of the flow direction to the North, which alters the path of the arriving air masses over the sea and, therefore, the evaporation and the moisture content. This might explain some of the variability in the CPs' reaction on temperature, especially in winter months when the energy input by radiation as driving force for convection is low.

Besides, daily temperatures do not capture all temperature dependent effect. The particularly high 99% quantile exceedance frequency during cold days of CP11 (Fig. 8e) is an example. CP11 leads to northern fluxes. If the atmosphere was warm before, the drop in temperature when the northern flux sets in releases much water due to the decreasing storage capacity of the air. The amount of released atmospheric water is rather a function of the temperature difference in this case and depends on the amount of available water that is present from the days before. For a more detailed classification, it could be beneficial to consider the temperature history before a precipitation event.

HESSD
10, 8841–8874, 2013

4 CP classification according to ECHAM5

4.1 Expected CP sequence

The CP-temperature classification will only give a valid prognosis for future precipitation if ECHAM5 is able to predict the CP sequence in a realistic manner. For a comparison with observations the CP defining rule set is applied to gridded MLSP data from the ECHAM5 20th century run. Figure 9 presents CP-frequencies of cyclonic and anticyclonic CPs between 1961 and 2000 according to the ECHAM5 simulation. The results derived from the NCEP/NCAR reanalysis (Fig. 5) are seen as a reference for the observed CP sequence. Since the 20th century run is a free simulation (except for the CO_2 forcing), it cannot be expected that the absolute frequencies according to ECHAM5 are the same as in the reanalysis data. In average over several years, however, the frequencies should be comparable and the trend signals similar if the GCM gives a valid representation of the atmospheric circulation.

ECHAM5 reproduces the average frequencies of cyclonic and anticyclonic CPs correctly (Fig. 9), but has limited capacity to represent the observed trend signals. Between September and April the trend is underestimated (Fig. 9a), in summer months it is completely missed (Fig. 9b). For the anticyclonic CPs ECHAM5 models a decreasing trend from September to April (Fig. 9c) that cannot be seen in the reanalysis data. The observed decreasing trend in summer, on the other hand, is underestimated (Fig. 9d).

4.2 Expected trend in 1h precipitation amounts

It was shown that the CP sequence has been significantly changing during the last forty years. Anticyclonic and, thus, dry conditions have become more frequent. In the same time, atmospheric temperature has been rising, shifting the distribution of hourly precipitation amounts towards higher values. The question is, how the two trend signals are combining in the future.

HESSD
10, 8841–8874, 2013

The downscaling method described in Sect. 2.4 is applied to two data sets, from the 20th century run (1961 to 2000; left column in Fig. 10) and the scenario A1B run of ECHAM5 (2001 to 2060; right column in Fig. 10). Based on the expected distributions of each year, the yearly sums (first line in Fig. 10) and the exceedance frequency of the 95 and 99 % quantile during the calibration period from 1991 and 2003 (second and third line in Fig. 10) are calculated. Since the calculation of the 95 % (99 %) quantile for the calibration period is based on wet hour only ($R \geq 0.1$ mm), the expected exceedance probabilities in respect to *all hours* in the year is lower than 5 % (1 %). An additional analysis is performed considering only the summer months from May to August (Fig. 11). Potential trends are estimated by linear regression, marked by a line in the respective diagramm. "Alpha" is the significance in a two sided hypothesis test of rejecting the hypothesis that the slope of the true regression line is zero.

The CP-temperature sequence derived from ECHAM5 consists of drier CP-temperature classes than the observed sequence. The expected yearly sums spread around 600 mm per year during the 20th century and the scenario run (Fig. 10a and b). The observed average over the 30 precipitation station used for calibration is about 150 mm higher. The expected yearly sums vary within a realistic range of 160 mm during the 20th century and the scenario run and exhibit no significant trend. The exceedance probabilities of the 95 and 99 % quantile of the calibration period, on the other hand, are increasing with time. The trend signal is strongest in the exceedance probability of the 99 % quantile during the scenario run, which is increasing by almost 20 % between 2000 and 2060 and with a very strong significance of $\alpha < 1$ %.

The trend signals in the exceedance probabilities of the 20th century run and the scenario run correspond well. The slopes of the linear regression function in both periods do not differ by more than some percent. The absolute values, however, are discontinuous. At the break point between 20th century and scenario run, from 2000 to 2001, the probabilities drop again to the level of 1960 to start increasing anew. Only in the precipitation sum, the end of the regression function of the control period is close to the starting point for the future period. Since the empirical histograms used for the cal-

HESSD
10, 8841–8874, 2013

culation are constant, it indicates a break point in the CP-temperature sequence and, thus, in the atmospheric circulation or the temperature data between the 20th century and the scenario run.

The summer months between May and August are predicted to become dryer (Fig. 11a and b), which indicates a shift of the precipitation activity towards winter. Nevertheless, the exceedance probabilities of the 95 and 99 % quantiles from the calibration period are still increasing during summer. The increase is strongest in the 99 % quantile (Fig. 11e and f), which is a result of a shift in the distribution towards the highest hourly precipitation amounts. Although it will rain less according to ECHAM5, it will rain more heavily. Again, the regression lines between the 20th century run and the A1B scenario run are discontinuous.

5 Conclusions

An objective, automated CP classification was set up that divides all days according to their distribution of the hourly precipitation sums. The CPs were further subdivided according to the atmospheric temperature. The results of the CP-temperature classification correspond well to physical considerations. During summer months, when convection plays a major role in precipitation genesis, there is a strong reaction to atmospheric temperature. On hot days it rains less frequent, but the frequency of extreme intensities is nevertheless higher. The reaction also depends on the CP. Anticyclonic CPs exhibit strong enhancement of extremes. CPs with western fluxes, leading to frontal rainfall, show the lowest enhancement. Outside the main convective season, from September to April, the reaction on temperature is less pronounced and more varying between the CPs. An increase in precipitation with higher temperature, which would be indicated by the Clausius–Clapeyron relation, could not be observed for all CPs. Probably, the CP-temperature classification is not able to completely separate the effect of circulation and temperature. Slight changes in atmospheric circulation also affect temperature, but do not necessarily change the CP class.

HESSD
10, 8841–8874, 2013

The CP-temperature classification is used as a spatial-temporal downscaling scheme for a prognosis of sub-daily precipitation in the future derived from large scale atmospheric circulation and temperature. It implies two major assumptions: Firstly, that ECHAM5 is able to predict the CP sequence of the future in a realistic manner and, secondly, that the precipitation distribution of each CP-temperature class is constant over time, which means that changes in the CP sequence and atmospheric temperature fully explain the changes in precipitation.

The capacity of ECHAM5 to represent the "true" CP sequence is limited. The CP frequencies are realistically modeled compared to the CP sequence based on NCEP/NCAR reanalysis data. Observed trends, however, e.g. an increase in high pressure situations during summer months, are missed. With the given data it cannot be judged if the differences between observed and simulated CP series are due to model errors. The verification period of forty years is too short to exclude that the deviations are merely a result of the different representation of inter-decennial variability between NCEP/NCAR and ECHAM5. The second assumption cannot be verified either. The temperatures in the future will most probably exceed the observed temperature range leading to new situations that have not yet occurred in the past. Therefore, the statistical response of all CPs during "hot" days may change. In this case, the second assumption is not valid any more. The same is true if climate change alters the atmospheric circulation resulting in CPs that have not been observed during the calibration period.

A clear problem of ECHAM5 is the inconsistency between the 20th century and the A1B scenario run. In most of the statistics, there is a pronounced jump between the two ECHAM5 runs. Probably, the results of the years 1961 to 2000 do not exhibit the same bias and model errors as the results of the years 2001 to 2060, which makes the interpretation difficult. If both data sets are regarded as one 100 yr long time series, no significant trend signals are found. The increase during the single runs is canceled by the jump at the break point between 2000 and 2001. The discontinuity is an indication of systematic differences between the two model runs, e.g. in the GCM's parametrization.

HESSD
10, 8841–8874, 2013

On the other hand, a recent study revealed that the internal stochastic variability concerning precipitation of climate models can attained a similar range as the difference between climate models (Deser et al., 2012). If the MSLP fields are to the same extend affected by internal variability, the jump could arise from pure random effects. However, MSLP data from GCM are regarded as more reliable than precipitation (Kendon and Clark, 2008).

In this study, the developed downscaling method is applied to a set of thirty rainfall stations that represent the average conditions of an area of about 35 000 km^2. With the same methodology it is also possible to provide precipitation data on the local scale if the empirical histograms are calculated for one single rainfall station. However, the restriction to one single location introduces a higher sampling uncertainty as the empirical precipitation frequencies of each CP-temperature combination are much lower. Since a stable estimation of the empirical histograms to each CP-temperature combination is crucial for the performance, the time series used for calibration have to be much longer and the number of CPs should be reduced, e.g. by regrouping the CP-temperature classes according to similarities in the empirical distributions. A regroupement into seven classes was tested by the given regional data and did not significantly affect the main findings.

Although the implicit assumptions and possible model errors are leading to high uncertainty in terms of the absolute trend signal, we have confidence in the general trend direction. The shift of precipitation from summer to winter is consistent with observed trends (Hundecha and Bárdossy, 2005) and confirmed by a direct analysis of RCM precipitation (Déqué et al., 2007). The predicted increase in extreme precipitation and the related shift in scaling towards more intensive short term events pursues a trend that has been observed in past data (Beck, 2013) and is consistent with physical considerations (Trenberth, 1999).

If the predictions are right, it will have severe consequences for all domains in which short term precipitation intensities play a major role. Besides urban hydrology with small catchments and fast response times, agricultural production will be severely af-

HESSD
10, 8841–8874, 2013

fected. The lower precipitation volume during summer months in combination with increased evaporation due to higher temperatures will augment the risk of water stress. Simultaneously, the probability for extreme precipitation intensities is increasing which means that crops will be damaged more frequently during rain storm events. For farmers this is problematic. They face a higher effort for irrigation in combination with more frequent losses of income due to bad harvests.

6 Outlook

The adaptation of sewage network design on future climate conditions would require complete future rainfall time series in hourly temporal resolution that can be fed to hydraulic channel models. The derived expected distributions of hourly rainfall sums are only the first step in this task. Next, it is intended to include the projections that were developed in this study in the data driven time series generator "NiedSim" (Bárdossy, 1998), which is used by the authorities of several federal states of Germany. NiedSim is a two step simulation that first sets up an initial time series by drawing from a theoretical distribution and then optimizes the order of values according to statistical target values like the autocorrelation on different lags or the scaling characteristics that are derived from observed precipitation time series. The generator makes as few conceptual assumption as possible and, instead, evaluates the time series by its appearance. Therefore, the distribution function defining the initial time series can be changed without affecting other properties, which makes it easy to incorporate future climate projections. In such a manner, the expected future distributions of hourly precipitation are going to be used for the set-up of the initial time series. The predicted changes in rainfall frequency during summer months or an assumed change in scaling could be modeled explicitly by altering the statistical target values of the optimization.

Acknowledgements. This work was kindly supported by the Landesanstalt für Umwelt, Messungen und Naturschutz Baden-Württemberg (LUBW) as well as by the German Research Foundation (DFG) within the funding programme Open Access Publishing.

HESSD
10, 8841–8874, 2013

References

Aarts, E. and van Laarhoven, P.: Simulated annealing: an introduction, Stat. Neerl., 43, 31–52, 1989. 8848

Bárdossy, A.: Generating precipitation time series using simulated annealing, Water Resour. Res., 34, 1737–1744, 1998. 8860

Bárdossy, A.: Atmospheric circulation patterns classification for southwest Germany using hydrolodical variables, Phys. Chem. Earth, 35, 498–506, 2010. 8847

Beck, F.: Generation of spatially correlated synthetic rainfall time series in high temporal resolution: a data driven approach, Ph.D. thesis, available at: http://elib.uni-stuttgart.de/opus/volltexte/2013/8216, Universität Stuttgart, Stuttgart, 2013. 8845, 8859

Berne, A., Delrieu, G., Creutin, J.-D., and Obled, C.: Temporal and spatial resolution of rainfall measurements required for urban hydrology, J. Hydrol., 299, 166–179, 2004. 8842

Déqué, M., Rowell, D., L uthi, D., Giorgi, F., Christensen, J., Rockel, B., Jacob, D., Kjellstr om, E., de Castro, M., and van den Hurk, B.: An intercomparison of regional climate simulations for Europe: assessing uncertainties in model projections, Climatic Change, 81, 53–70, doi:10.1007/s10584-006-9228-x, 2007. 8844, 8859

Deser, C., Phillips, A., Bourdette, V., and Teng, H.: Uncertainty in climate change projections: the role of internal variability, Clim. Dynam., 38, 527–546, 2012. 8859

Fowler, H. J., Ekström, M., and Blenkinsop, S.: Estimating change in extreme European precipitation using a multimodel ensemble, J. Geophys. Res., 112, D18104, doi:10.1029/2007JD008619, 2007. 8844

Groppelli, B., Bocchiola, D., and Rosso, R.: Spatial downscaling of precipitation from GCMs for climate change projections using random cascades: a case study in Italy, Water Resour. Res., 47, W03519, doi:10.1029/2010WR009437, 2011. 8844

Guichard, F., Petch, J. C., Redelsperger, J.-L., Bechtold, P., Chaboureau, J.-P., Cheinet, S., Grabowski, W., Grenier, H., Jones, C. G., Köhler, M., Piriou, J.-M., Tailleux, R., and Tomasini, M.: Modelling the diurnal cycle of deep precipitating convection over land with cloud-resolving models and single-column models, Q. J. Roy. Meteorol. Soc., 130, 3139–3172, 2004. 8844

Held, I. M. and Soden, B. J.: Robust responses of the hydrological cycle to global warming, J. Climate, 19, 5686–5699, 2006. 8843

HESSD
10, 8841–8874, 2013

Hundecha, Y. and Bárdossy, A.: Trends in daily precipitation and temperature extremes across western Germany in the second half of the 20th century, Int. J. Climatol., 25, 1189–1202, 2005. 8844, 8859

Kendon, E. and Clark, R.: Reliability of future changes in heavy rainfall over the UK, in: BHS 10th National Hydrology Symposium, Exeter, 2008. 8846, 8859

Kendon, E., Rowell, D., and Jones, R.: Mechanisms and reliability of future projected changes in daily precipitation, Clim. Dynam., 35, 489–509, doi:10.1007/s00382-009-0639-z, 2010. 8843

Kistler, R., Kalnay, E., Collins, W., Saha, S., White, G., Woollen, J., Chelliah, M., Ebisuzaki, W., Kanamitsu, M., Kousky, V., van den Dool, H., Jenne, R., and Fiorino, M.: The NCEP–NCAR 50-year reanalysis: monthly means CD-ROM and documentation, B. Am. Meteorol. Soc., 82, 247–268, 2001. 8847

Lenderink, G. and van Meijgaard, E.: Increase in hourly precipitation extremes beyond expectations from temperature changes, Nat. Geosci., 1, 511–514, 2008. 8845

Lenderink, G., Buishand, A., and van Deursen, W.: Estimates of future discharges of the river Rhine using two scenario methodologies: direct versus delta approach, Hydrol. Earth Syst. Sci., 11, 1145–1159, doi:10.5194/hess-11-1145-2007, 2007. 8845

Lenderink, G., Mok, H. Y., Lee, T. C., and van Oldenborgh, G. J.: Scaling and trends of hourly precipitation extremes in two different climate zones – Hong Kong and the Netherlands, Hydrol. Earth Syst. Sci., 15, 3033–3041, doi:10.5194/hess-15-3033-2011, 2011. 8845

Molnar, P. and Burlando, P.: Preservation of rainfall properties in sthochastic disaggregation by a simple random cascade model, Atmos. Res., 77, 137–151, 2005. 8844

Nguyen, V.-T.-V., Nguyen, T.-D. and Cung, A.: A statistical approach to downscaling of sub-daily extreme rainfall processes for climate-related impact studies in urban areas, Water Sci. Technol., 7, 183–192, 2007. 8844

Roeckner, E., Bäuml, G., Bonaventura, L., Brokopf, R., Esch, M., Giorgetta, M., Hagemann, S., Kirchner, I., Kornblueh, L., Manzini, E., Rhodin, A., Schlese, U., Schulzweida, U., and Tompkins, A.: The Atmospheric General Circulation Model ECHAM5, Tech. rep., Max-Planck-Institut für Meteorologie, Hamburg, Germany, 2003. 8850

Trenberth, K. E.: Conceptual framework for changes of extremes of the hydrological cycle with climate change, Climatic Change, 42, 327–339, doi:10.1023/A:1005488920935, 1999. 8854, 8859

Trenberth, K. E., Dai, A., Rasmussen, R. M., and Parsons, D. B.: The changing character of precipitation, B. Am. Meteorol. Soc., 84, 1205–1217, 2003. 8844, 8846

HESSD
10, 8841–8874, 2013

Wentz, F. J., Ricciardulli, L., Hilburn, K., and Mears, C.: How much more rain will global warming bring?, Science, 317, 233–235, 2007. 8843
Willems, P. and Vrac, M.: Statistical precipitation downscaling for small-scale hydrological impact investigations of climate change, J. Hydrol., 402, 193–205, 2011. 8845

HESSD
10, 8841–8874, 2013

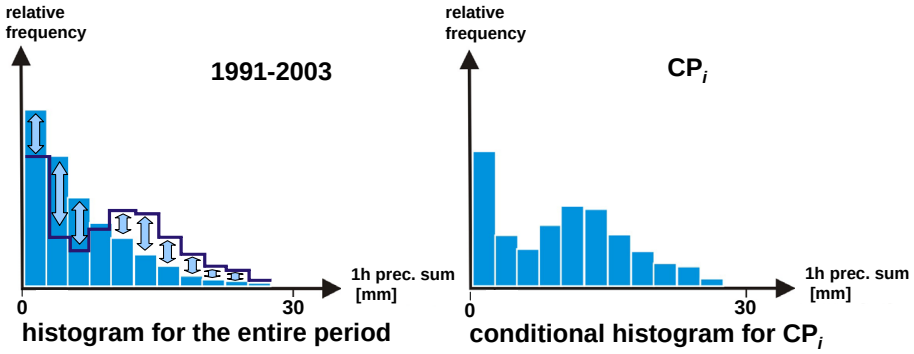

Fig. 1. Principle of the objective function for the CP definition in the simulated annealing scheme.

HESSD
10, 8841–8874, 2013

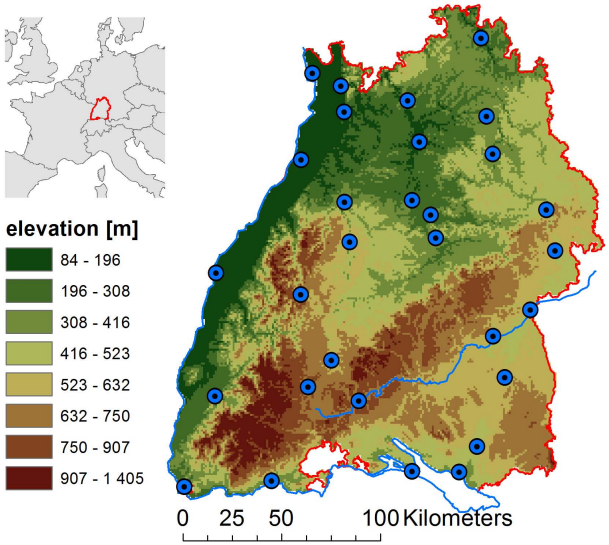

Fig. 2. Set of 30 high resolution rain gauges with continuous measurements from 1991 to 2003 and low number of missing values.

HESSD
10, 8841–8874, 2013

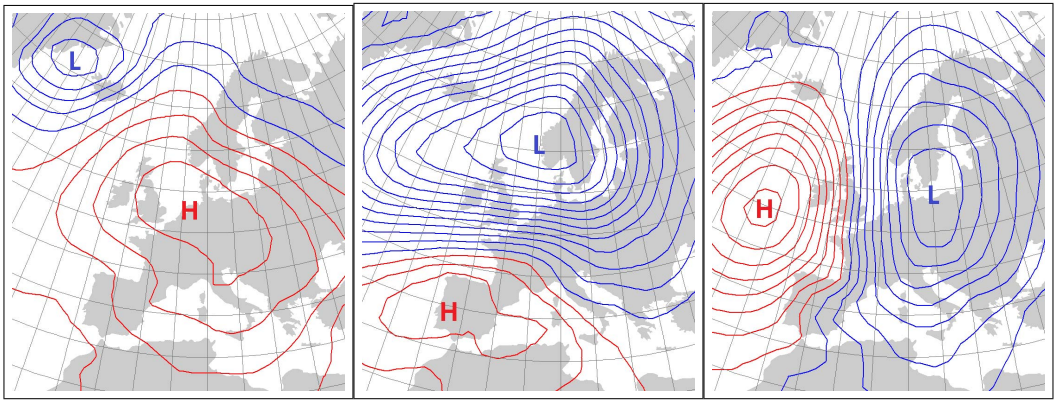

(a) CP2 (b) CP7 (c) CP11

Fig. 3. 1 hPa isobars of mean sea level pressure anomalies of CPs related to high precipitation intensities.

HESSD
10, 8841–8874, 2013

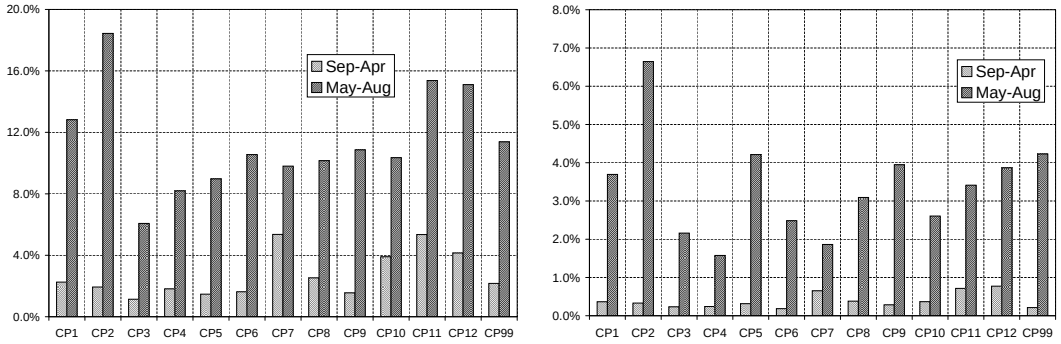

(a) 95 % quantile

(b) 99 % quantile

Fig. 4. Exceedance frequency of the 95 and 99 % quantile for two seasons; quantiles and frequencies are calculated for all hours with $R \geq 0.1$ mm.

HESSD
10, 8841–8874, 2013

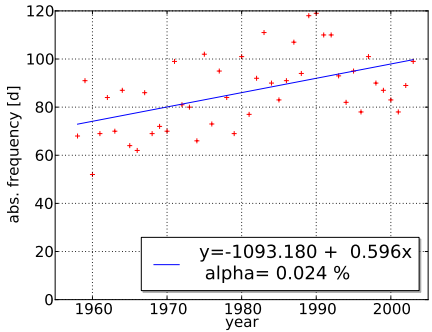

(a) Anticyclonic CPs - September to April

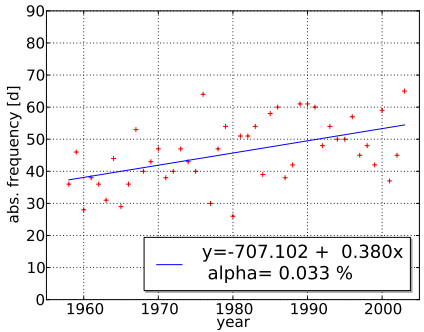

(b) Anticyclonic CPs - May to August

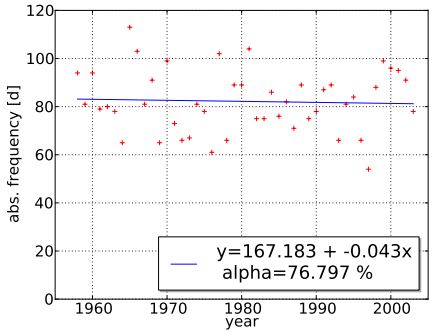

(c) Cyclonic CPs - September to April

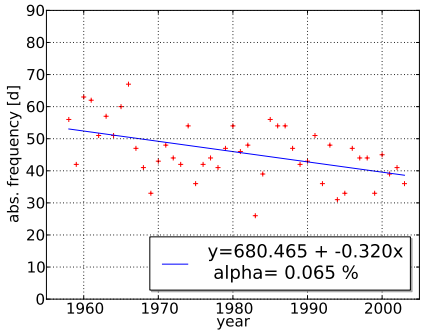

(d) Cyclonic CPs - May to August

Fig. 5. Trends in the frequency of anticyclonic (first line) and cyclonic CPs (second line) according to NCEP/NCAR reanalysis.

HESSD
10, 8841–8874, 2013

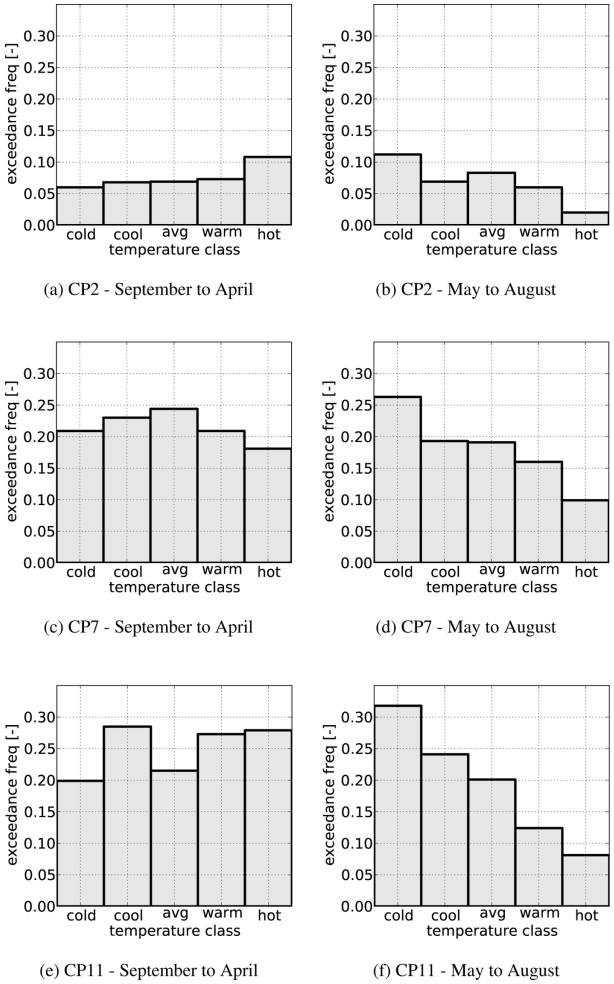

(a) CP2 - September to April

(b) CP2 - May to August

(c) CP7 - September to April

(d) CP7 - May to August

(e) CP11 - September to April

(f) CP11 - May to August

Fig. 6. Frequency of $R \geq 0.1$ mm according to three different CPs and two seasons.

HESSD
10, 8841–8874, 2013

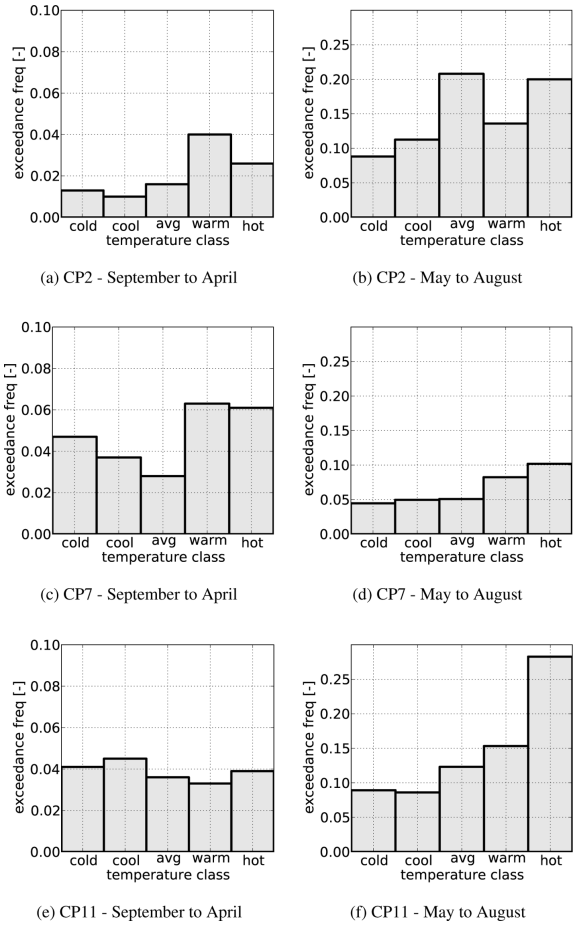

Fig. 7. Exceedance frequency of the 95% quantile according to three different CPs and two seasons; the exceedance frequency referrs to all hours with $R \geq 0.1$ mm.

HESSD
10, 8841–8874, 2013

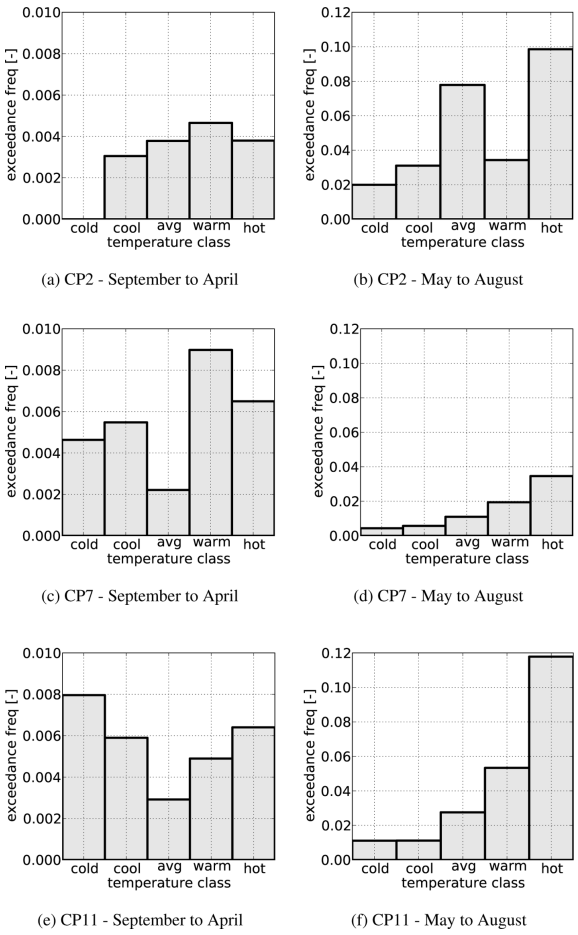

Fig. 8. Exceedance frequency of the 99 % quantile according to three different CPs and two seasons; the exceedance frequency referrs to all hours with $R \geq 0.1$ mm.

HESSD
10, 8841–8874, 2013

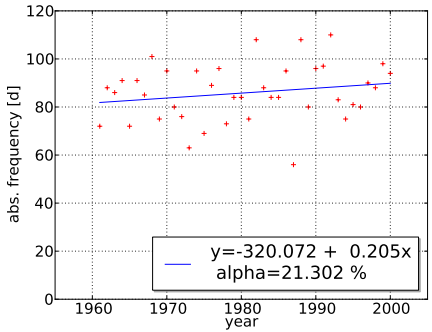

(a) ECHAM5 - September to April

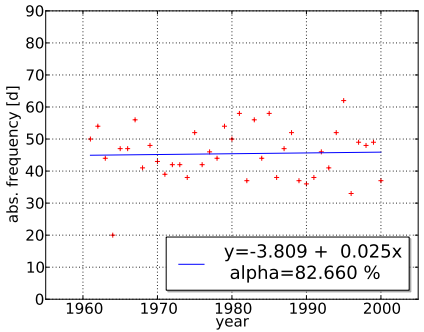

(b) ECHAM5 - May to August

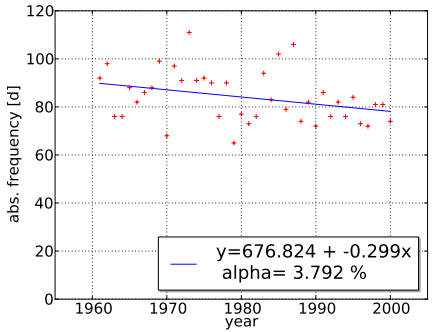

(c) ECHAM5 - September to April

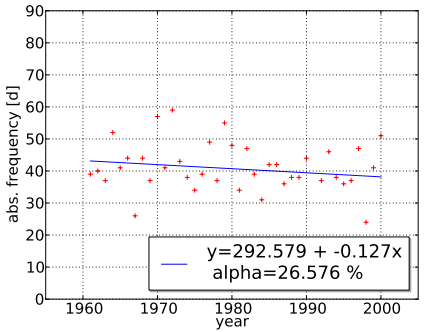

(d) ECHAM5 - May to August

Fig. 9. Trends in the frequency of anticyclonic (first line) and cyclonic CPs (second line) according to the 20th century run of ECHAM5 during two seasons.

HESSD
10, 8841–8874, 2013

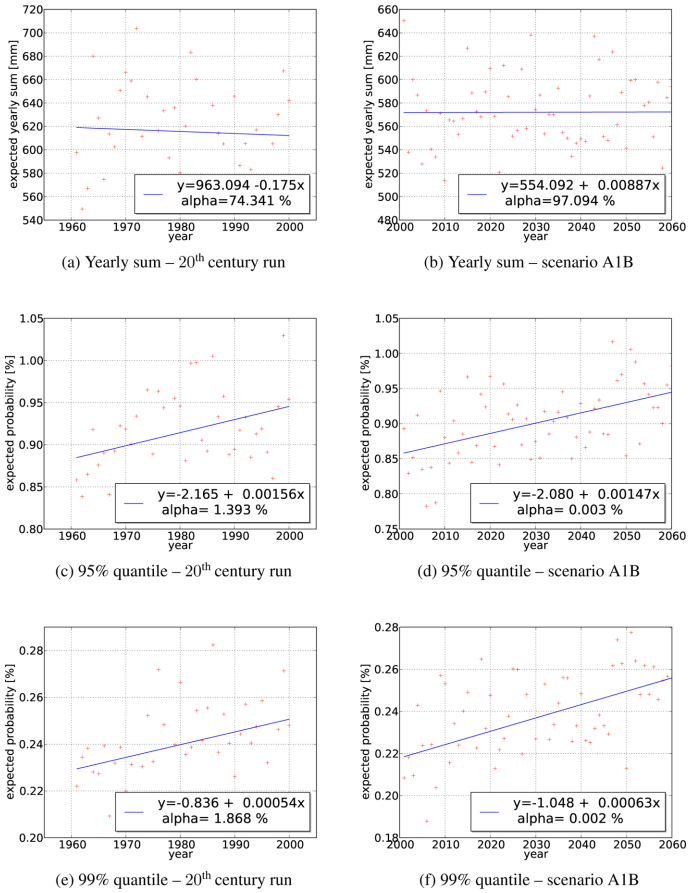

Fig. 10. Linear trend in the expected yearly precipitation sum and the probability of hourly values exceeding the 95 and 99 % quantile of the calibration period according to the CP-temperature sequence derived from ECHAM5.

HESSD
10, 8841–8874, 2013

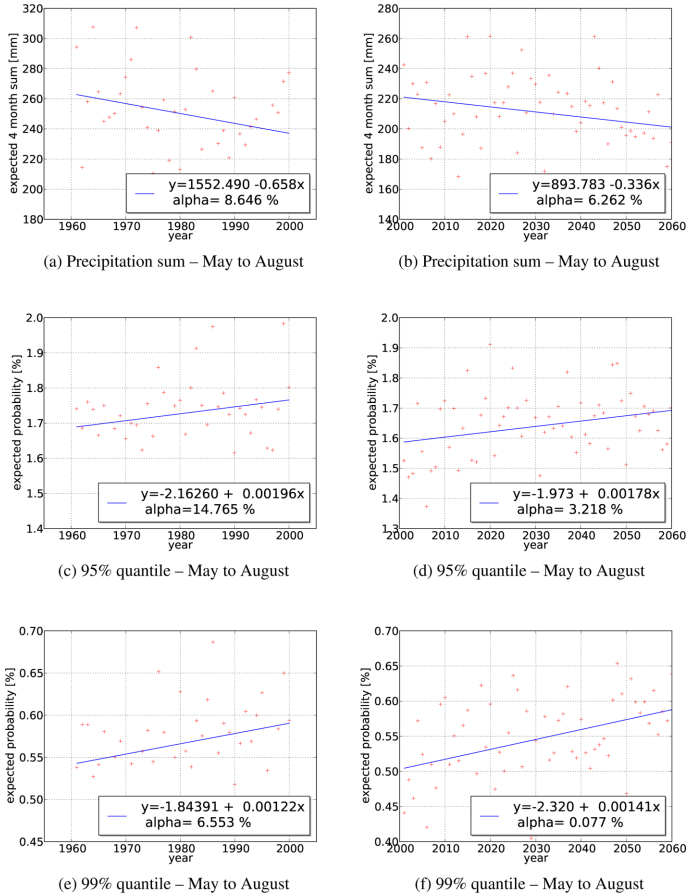

Fig. 11. Linear trend during summer months in the expected precipitation sum and the yearly probability of values exceeding the 95 and 99 % quantile of the calibration period according to the CP-temperature sequence derived from ECHAM5's 20th century and scenario A1B run.

HESSD
10, 8841–8874, 2013